Sensitivity of Precipitation Statistics to Resolution, Microphysics, and Convective Parameterization: A Case Study with the High-Resolution WRF

Sensitivity of Precipitation Statistics to Resolution, Microphysics, and Convective Parameterization: A Case Study with the High-Resolution WRF Climate Model over Europe

ALEXANDRE B. PIERI AND JOST VON HARDENBERG

Institute of Atmospheric Sciences and Climate, National Research Council, Turin, Italy

ANTONIO PARODI

CIMA Foundation, Savona, and Institute of Atmospheric Sciences and Climate, National Research Council, Turin, Italy

ANTONELLO PROVENZALE

Institute of Atmospheric Sciences and Climate, National Research Council, Turin, and Institute of Geosciences and Earth Resources, National Research Council, Pisa, Italy

(Manuscript received 19 November 2014, in final form 23 February 2015)

ABSTRACT

We explore the impact of different resolutions, convective closures, and microphysical parameterizations on the representation of precipitation statistics (climatology, seasonal cycle, and intense events) in 20-yr-long simulations over Europe with the regional climate Weather Research and Forecasting (WRF) Model. The simulations are forced in the period 1979–98, using as boundary conditions the ERA-Interim fields over the European region. Special attention is paid to the representation of precipitation in the Alpine area. We consider spatial resolutions ranging from 0.11° to 0.037°, allowing for an explicit representation of convection at the highest resolution. Our results show that while there is a good overall agreement between observed and modeled precipitation patterns, the model outputs display a positive precipitation bias, particularly in winter. The choice of the microphysics scheme is shown to significantly affect the statistics of intense events. High resolution and explicitly resolved convection help to considerably reduce precipitation biases in summer and the reproduction of precipitation statistics.

1. Introduction

Precipitation is one of the most crucial meteorological and climatological variables affecting environmental conditions and human societies. In particular, estimating the expected impact of climate change on hydrometeorological risk, ecosystem functioning, permafrost thawing, snow and glacier melt, and water availability requires quantitative and precise precipitation estimates with high spatial and temporal resolution (Giorgi 2006; Fowler and Wilby 2010). This requirement is particularly stringent when considering flood risk assessment in mountain or coastal basins with moderate spatial extension (Rebora et al. 2006).

While global climate models (GCMs) are currently reaching higher and higher resolutions, they are still limited to scales of the order of 50–100 km [as in phase 5 of the Coupled Model Intercomparison Project (CMIP5)], thus presenting a large gap between the scales reproduced by the model and the scales of interest for most of the processes involving precipitation and its impacts (such as flood and landslides). To try to circumvent this difficulty, regional climate models (RCMs) nested into GCMs are used to dynamically downscale GCMs and achieve both higher resolution and a better and more physically based representation of the small-scale processes (Giorgi 1990, 2006; Giorgi and Mearns 1991; McGregor 1997; Castro et al. 2005). Investigations of the limits of such methods are found in Denis et al. (2002) and Vannitsem and Chomé (2005). While the resolution of RCMs has increased in the course of time, using nested RCMs still presents issues such as the

Corresponding author address: Alexandre B. Pieri, Institute of Atmospheric Sciences and Climate, National Research Council, Corso Fiume 4, 10133 Turin, Italy.
E-mail: a.pieri@isac.cnr.it

DOI: 10.1175/JHM-D-14-0221.1

influence of boundary conditions, the best size of the nested domains, and the choice of adequate parameterizations, all of which can severely affect the simulated precipitation output. In particular, the added value provided by very high horizontal resolution of precipitation fields in regional climate simulations remains unclear (Chan et al. 2014). For example, Prein et al. (2013) showed, using the Weather Research and Forecasting (WRF) Model, that grid spacing of at least 6 km was needed to faithfully reproduce the spatial pattern and amount of precipitation in experiments over the Colorado basin. In general, as underlined by the fifth assessment report of the IPCC, regional modeling of precipitation still needs strong improvements in order to reach a robust confidence interval. Therefore, a careful analysis of the sensitivity of the model response to different parameterizations such as spatial resolution, microphysics, and convective schemes is an essential step before embarking on the use of model outputs to assess the impact of climate change.

In this framework, Europe represents an especially challenging region for modeling precipitation, since it is exposed to intense synoptic perturbations from the Atlantic and to moisture-rich inflows from the Mediterranean and is characterized by complex orographic features. Climatology of the European region is complex and at least four climate subregions can be identified: humid temperate climate (western Europe), humid cold climate (eastern Europe), Mediterranean climate, and Alpine climate. Dynamical downscaling of climate change scenarios have shown that wet regions will probably be shifted northward while experiencing increased magnitude and frequency of extreme precipitation events (Christensen and Christensen 2003; Frei et al. 2006). Hence, a better understanding of the internal variability of the models and their sensitivity to tuning parameters and parameterizations is of main interest in order to derive significant conclusions in this region. Several efforts in regional dynamical downscaling over Europe have been made in the past decades (see, e.g., Giorgi et al. 1990; Jones et al. 1995; Wilson and Mitchell 1987). For a general discussion on dynamical downscaling over Europe, see Murphy (2000). More recently, an important endeavor to achieve finer-scale climate prediction over Europe has been performed in the framework of the Coordinated Regional Climate Downscaling Experiment (CORDEX; Chu et al. 2010; Gobiet et al. 2012; Warrach-Sagi et al. 2013; Jacob et al. 2013; Flaounas et al. 2013). An evaluation of the European CORDEX ensemble performance is reported in Kotlarski et al. (2014).

In this work, we explore the role of different microphysical parameterizations and convective closures for a state-of-the-art regional climate model, the WRF Model, applied to the European domain defined in CORDEX and run at different spatial resolutions down to 0.037° (~4 km), comparing the model results with the observed precipitation properties provided by a number of available observational and reanalysis datasets. In particular, we focus our analysis on the rainfall distribution over the greater Alpine region (GAR) as a representative region characterized by complex topography, where orographic lifting plays an important role (Roe 2005; Rotunno and Houze 2007).

Monthly and daily statistics obtained from the model for the period 1979–98 are compared with the observational data in order to determine the best configuration for reproducing precipitation climatology, particularly in the Alpine region and including the statistics of intense precipitation occurrences, and to assess strengths and weaknesses of the modeling approaches.

The paper is organized as follows. In section 2 we introduce the numerical model, the study area, and the observational datasets that are used to test our numerical results. Section 3 describes the numerical experiments performed, which differ from each other in terms of resolution, microphysics, and convective parameterizations. A comparative study of different parameterizations is then provided. Section 4 discusses the numerical results, focusing particularly on the spatial distribution of yearly average precipitation, the reproduction of the seasonal cycle, and the statistics of daily precipitation. Discussion and conclusions are reported in section 5.

2. Model, simulation domains, and observational datasets

We use the Advanced Research version of WRF (ARW), version 3.4.1, which is a nonhydrostatic, compressible, and scalar-conserving state-of-the-art atmospheric model (Skamarock et al. 2005). Recent applications of the WRF Model as a nested RCM for dynamical downscaling can be found in Lo et al. (2008) and Bukovsky and Karoly (2009).

The area of study used for model integration is the European domain defined in CORDEX (Jacob et al. 2013). This represents an area defined in an equidistant latitude–longitude projection with rotated North Pole, extending approximately in the range 27°–72°N latitude and 22°W–45°E longitude (centers of the boundaries). For the high-resolution run, we use a two-way nested strategy defining an inner region [which we call the inner European region (IER) in the following]. This allows us to avoid abrupt changes in the resolution between the forcing dataset (ERA-Interim; 0.75°) and the numerical model. Finally, we define a smaller region corresponding

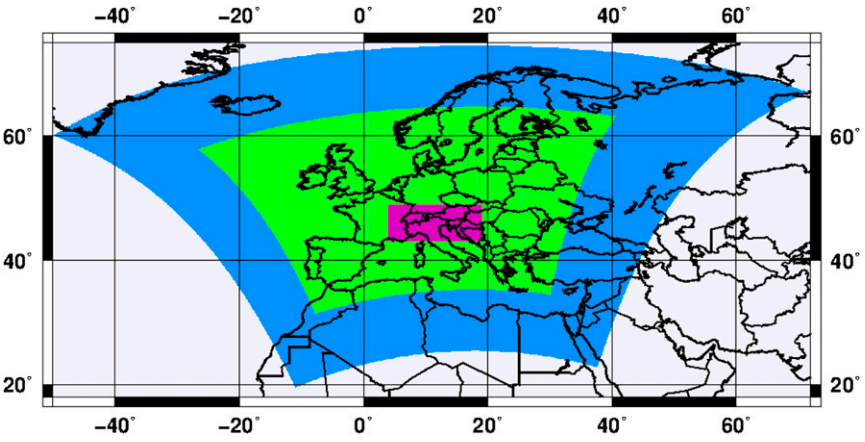

FIG. 1. The European domain defined in CORDEX (0.11°; blue) and the IER (0.037°; green) used for the high-resolution integration. The GAR used for some of the diagnostics is displayed in purple.

to the GAR, extending in the range 43°–49°N latitude and 4°–19°E longitude; we use this latter region to compare model runs with observations over the Alpine region. The various domains are reported in Fig. 1.

Model precipitation is compared with a range of observational and reanalysis datasets available for the period 1979–98: the ERA-Interim dataset (Dee et al. 2011), the Modern-Era Retrospective Analysis for Research and Applications (MERRA; Rienecker et al. 2011; Saha et al. 2010; Wang 2011), the Global Precipitation Climatology Centre (GPCC) dataset (Becker et al. 2013), the Climatic Research Unit (CRU) dataset (New et al. 1999, 2000), and the European daily high-resolution gridded dataset (E-OBS; Haylock et al. 2008). For the GAR domain, we also consider the Historical Instrumental Climatological Surface Time Series of the Greater Alpine Region (HISTALP) precipitation dataset (Auer et al. 2007) and the more recent high-resolution Alpine precipitation grid dataset (APGD) developed by MeteoSwiss in the framework of the European Reanalysis and Observations for Monitoring (EURO4M) collaborative project (Isotta et al. 2013). Table 1 summarizes the characteristics of these datasets. In all cases, the datasets provide gridded precipitation estimates that can be (even severely) affected by the method used to generate a regular grid of precipitation values from sparse rain gauge observations; see, for example, Palazzi et al. (2013) for an illustration of this problem in the Himalaya–Karakoram region. Thus, although we take the different gridded precipitation datasets as possible realizations of a "ground truth," uncertainties exist also on the observational side.

For the comparison between data and model outputs, when the observations have much lower resolution, unless otherwise specified the higher-resolution precipitation fields produced by the numerical simulations are remapped to the resolution of the gridded dataset under consideration using bilinear interpolation.

3. Numerical simulations

The WRF Model includes a wide range of possible parameterizations. Here, we focus mainly on changes in the microphysical and in the cumulus convection parameterization schemes, also considering explicitly resolved convection in a high-resolution simulation, and aim at assessing the model performance in terms of precipitation climatology, statistics, and extremes.

TABLE 1. Acronyms and characteristics of the observational and reanalysis datasets used in this study. Abbreviations: time series (TS), Deutscher Wetterdienst (DWD), and Zentralanstalt für Meteorologie und Geodynamik (ZAMG).

Name	Version	Grid	Institution	Data type	Reference
ERA-Interim		0.75° × 0.75°	ECMWF	Reanalysis	Dee et al. (2011)
MERRA	GEOS-5.2.0	0.67° × 0.5°	NASA EOS	Reanalysis	Rienecker et al. (2011)
GPCC	5	0.5° × 0.5°	DWD	Observation	
E-OBS	7.0	0.25°	E-OBS	Observation	Haylock et al. (2008)
CRU	TS 3.01.01	0.5°	CRU	Observation	Mitchell and Jones (2005)
HISTALP		0.083°	ZAMG	Observation	Auer et al. (2007)
EURO4M-APGD		5 km	EURO4M	Observation	Isotta et al. (2013)

Although obtained using a specific model, this approach helps understanding what are the most important points to be considered in high-resolution precipitation simulations on climatic time scales.

We perform numerical experiments at different spatial resolutions, varying from 0.11° to 0.037°. In the case of the high-resolution simulation, the model is run at 0.037° in the internal domain and at 0.11° in the external domain, adopting a two-way nesting. In this case, the solution in the nested domain feeds back on the coarse-grid solution. The time step is fixed to 45 s for the coarse grid and to 15 s for the fine grid. The boundary conditions are specified by the parent grid at every coarse-grid time step. Owing to the numerical weight of the simulations, we focus on a specific 20-yr-long period, namely, the period 1979–98. Lateral boundary conditions, sea surface temperatures, and sea ice coverage for our experiments are provided by the ERA-Interim data (Dee et al. 2011) for the whole period 1979–98. ERA-Interim is also used to provide initial conditions to the WRF Model over the study domain, in particular providing an initial estimate of the surface parameters, soil humidity, and soil temperature (four layers).

The WRF simulations are performed as single runs over the whole period for the medium resolutions (0.11°). For the high-resolution run (0.037°), we split the period 1979–98 into several 3-yr-long subperiods, which are run in parallel. The first subperiod starts on 1 January 1979 and ends on 1 January 1982, and the others follow. Initial conditions, including soil moisture, are reset at the beginning of each subperiod to ERA-Interim fields. While this choice may have an impact on the model dynamics at the beginning of each new subperiod, we checked that the results presented in this paper are verified also when statistics are based only on years in which no initialization was performed. Continuity of the synoptic driver at the beginning of each new subperiod is assured by the boundary conditions provided by ERA-Interim (lateral and surface). Table 2 summarizes the details of all the simulations that were performed.

TABLE 2. Details and identification (ID) of the different numerical experiments performed with WRF. Within the experiment ID, convective schemes are indicated by a "k" for the KF scheme and a "b" for the BMJ scheme. Microphysics parameterizations are indicated by "t" for the Thompson scheme, "m" for the Morrison scheme, and "w" for WSM6. The last two integers indicate the horizontal resolution of the simulation.

Expt ID	Grid	Microphysics	PBL/convective scheme
kt11	0.11°	Thompson	KF
km11	0.11°	Morrison	KF
kws11	0.11°	WSM6	KF
bt11	0.11°	Thompson	BMJ
et04	0.037°	Thompson	Explicit

a. *Convection schemes and spatial resolution*

We investigate the sensitivity of the model to the convection scheme by considering the Kain–Fritsch CAPE removal time-scale closure (KF; Kain and Fritsch 1990) and the Betts–Miller–Janjic adjustment type closure (BMJ; Betts 1986) schemes. The KF parameterization is a mass-flux scheme, suitable for mesoscale models and able to handle very intense convection, designed to rearrange mass in a column so that CAPE is consumed. However, this parameterization may leave unrealistically deep saturated layers in postconvective soundings, causing in turn the microphysics scheme to be activated and oversimulating postconvective stratiform precipitation associated with synoptic-scale cloud systems (Gallus 1999). The BMJ is a profile-relaxation-type scheme adjusting the sounding toward a predetermined, postconvective reference profile derived from climatology. The BMJ scheme is only triggered for soundings with deep moisture profiles, and when triggered, the scheme often consumes available humidity too quickly, leaving too little water vapor behind for precipitation to occur later or downstream (Jankov et al. 2005); this explains a tendency of this convective closure toward too dry conditions, making it the most effective scheme in not overpredicting precipitation. A comparison of these schemes was performed in Wang and Seaman (1997), at resolutions down to 12 km for precipitation events over the continental United States, and the authors found the Kain–Fritsch scheme to be the better-performing one while showing that KF tends to overestimate light rain events when compared to BMJ. The Kain–Fritsch convective parameterization has been recently used for a sensitivity study of the WRF over the European domain in Mooney et al. (2013).

We compare the runs with parameterized convection to a high-resolution run with explicit convection at a resolution of 0.037°. In this case we use a two-way nesting, running WRF at the higher resolution in the limited inner nested IER area defined above and exchanging boundary conditions with the WRF simulation running in the external European domain defined in CORDEX at 0.11°. In the external domain, the Kain–Fritsch convective scheme is used. The finer resolution should make the model able to resolve explicitly, albeit crudely, convective processes (Kain et al. 2006, 2008). Some studies have investigated these so-called gray zone resolutions (Gerard 2007) to understand whether a convective parameterization can work correctly on such scales, but at the moment this is still an open question (Yu and Lee 2010).

TABLE 3. Averages over the IER domain, limited to land surfaces, of the average rainfall rate (mm day^{-1}) for the different observational datasets and the different WRF configurations used in the present study. The percentage differences from E-OBS are reported in parentheses.

Run	DJF	MAM	JJA	SON	Year
kt11	2.34 (34%)	2.67 (62%)	3.20 (66%)	2.50 (25%)	2.68 (46%)
km11	2.39 (37%)	2.50 (52%)	3.01 (56%)	2.50 (25%)	2.60 (42%)
kw11	2.42 (39%)	2.67 (62%)	3.15 (63%)	2.56 (28%)	2.70 (48%)
bt11	2.31 (33%)	2.46 (49%)	2.63 (36%)	2.29 (15%)	2.43 (33%)
et04	2.33 (34%)	2.28 (38%)	2.25 (17%)	2.29 (15%)	2.29 (25%)
ERA-Interim	1.80	1.93	2.33	1.99	2.01
CRU	1.71	1.71	2.12	2.00	1.89
E-OBS	1.74	1.65	1.93	2.00	1.83
GPCC	1.80	1.77	2.14	2.08	1.95
MERRA	1.74	1.75	2.09	1.86	1.86

b. *Microphysics*

We explore the role of microphysical parameterizations by comparing three different microphysical schemes: the WRF single-moment 6-class microphysics scheme (WSM6; Hong and Lim 2006), the Thompson et al. (2004) microphysics closure, and the Morrison and Gettelman (2008) scheme. These are all 6-class schemes that consider vapor, rain, snow, cloud ice, cloud water, and graupel and include the representation of mixed-phase processes, that is, interactions of ice and water particles such as riming. Of the three WRF single-moment (WSM) schemes available in WRF, WSM6 is recommended for cloud-resolving grids (Hong and Lim 2006). The Morrison and Gettelman (2008) scheme is a two-moment bulk microphysics scheme that, in addition to the mixing ratios, predicts independent number concentrations for ice, snow, rain, and graupel. The Thompson et al. (2004) scheme is a two-moment scheme as it also predicts number concentrations for ice and rain. This scheme produces larger amounts of snow at all levels with respect to WSM6, owing to enhanced cloud ice content in the upper troposphere (Otkin et al. 2006).

4. Results

a. *Rainfall climatology*

Tables 3 and 4 report the annual rainfall rate, averaged over the IER and over the GAR, respectively, for the different numerical experiments and the different observational datasets. Averages have been computed by weighting the original model/observational grid values (at the native resolution) by the fraction of each grid cell falling in the selected domain and limited to land surfaces (i.e., excluding seas and oceans). The tables also report absolute and percentage biases separated by season and the percentage difference between the simulations and E-OBS climatologies in the IER domain and between the simulations and the HISTALP dataset in the GAR domain. We find that all numerical simulations produce annual precipitation means that are significantly larger than those indicated by gridded precipitation datasets. The simulation using explicit convection (et04) is the only one with only 25% average excess precipitation with respect to E-OBS on the IER domain. In the GAR domain, the bias on climatology reduces to only 4.7% for this

TABLE 4. Averages over the GAR domain, limited to land surfaces, of the average rainfall rate (mm day^{-1}) for the different observational datasets and the different WRF configurations used in the present study. The percentage differences from HISTALP are reported in parentheses.

Run	DJF	MAM	JJA	SON	Year
kt11	2.83 (16%)	3.85 (36%)	4.56 (43%)	3.44 (4%)	3.67 (24%)
km11	2.97 (21%)	3.56 (26%)	4.37 (37%)	3.37 (2%)	3.57 (21%)
kw11	3.04 (24%)	4.00 (41%)	4.63 (46%)	3.49 (5%)	3.79 (28%)
bt11	2.99 (22%)	3.67 (30%)	3.50 (10%)	3.21 (4%)	3.34 (13%)
et04	2.76 (13%)	3.35 (18%)	3.10 (3%)	3.13 (6%)	3.09 (4.7%)
ERA-Interim	2.29	2.79	3.16	2.69	2.73
CRU	2.24	2.74	3.23	3.05	2.82
E-OBS	2.20	2.47	2.75	2.88	2.58
GPCC	2.21	2.60	3.03	2.96	2.70
MERRA	2.11	2.46	2.53	2.37	2.37
HISTALP	2.45	2.83	3.18	3.32	2.95

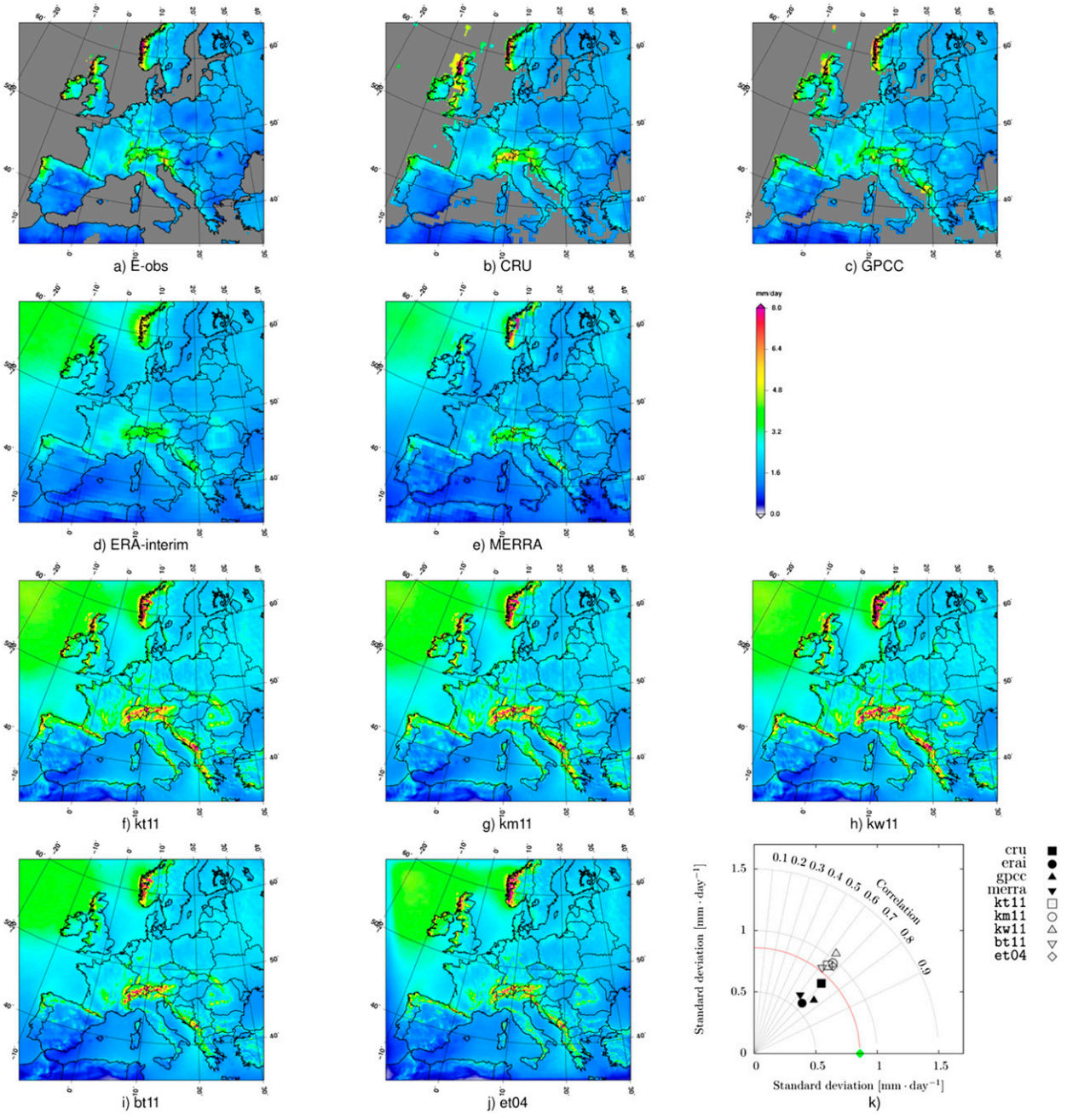

FIG. 2. Total precipitation rate averaged over the period 1979–98 for (a)–(e) observational datasets and (f)–(j) numerical experiments performed in this study. (k) The Taylor diagram corresponding to the various experiments and datasets; E-OBS was chosen as the reference.

simulation. For runs with parameterized convection (at 0.11°), those using KF all give biases above 42% for the IER region (above 21% in the GAR), while the run with BMJ convective closure (bt11) gives an excess precipitation of 33% in the IER (13% in the GAR).

The spatial distribution of precipitation, averaged over the whole period 1979–98, is shown in Figs. 2a–j. For all model runs (Figs. 2f–j), we find positive biases over all areas with complex topography when compared to observational datasets (reported in Figs. 2a–e). Common biases are an excessive rainfall rate over Croatia and the Pyrenees (except for runs bt11 and et04), excessive rainfall over the Alps and over northeastern Europe, and a positive bias ($\sim$3 mm day^{-1}) over

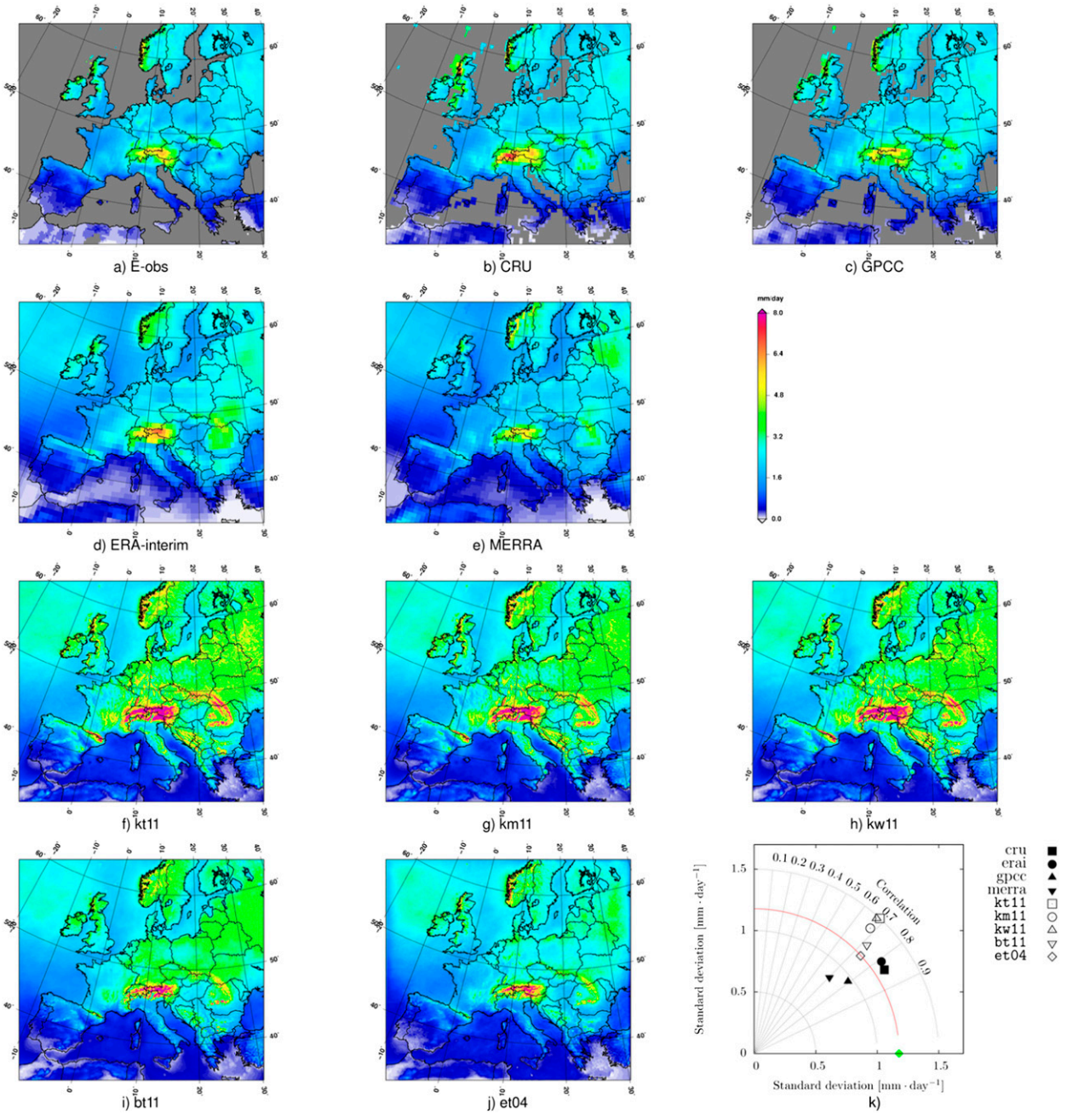

FIG. 3. As in Fig. 2, but for the nested domain during JJA.

the Carpathian Mountains. The high-resolution run (et04) in Fig. 2j displays a slightly better performance, reducing the excess precipitation over eastern Europe and the Alps. In evaluating these results, one has to take into account the uncertainties in the observational datasets. For example, the quality of E-OBS is limited over the Carpathian Mountains, the Pyrenees, and Croatia, owing to the very limited rain gauge density in these areas (Haylock et al. 2008).

Figure 3 shows the spatial distribution of precipitation averaged over the whole period 1979–98 for the summer [June–August (JJA)] season. Average precipitation over eastern Europe is overestimated by all WRF configurations for this particular season, independently on the convective parameterization. During the summer, runs kt11 and bt11 (Figs. 2f,i) exhibit a wet bias of $\sim 2\,\mathrm{mm\,day^{-1}}$ over eastern Europe while the high-resolution run et04 (Fig. 2j) is in better agreement with

the observed datasets. Hence, using explicit convection during summer, when the convective component of precipitation is dominant, helps to reproduce the precipitation patterns and to avoid spurious precipitation from the convective closure.

Taylor diagrams are used to provide a concise view of the model performances (see Figs. 2k, 3k). The reference dataset is E-OBS and all simulation datasets have been upscaled to its resolution for comparison. The distance from the origin indicates the standard deviation of the simulation/dataset and the solid red arc represents the standard deviation of E-OBS. The angle with the horizontal indicates the spatial correlation between E-OBS and the different simulations/datasets so that the best score in this metric would be a point lying on the intersection between the solid red arc and the horizontal. For the annual climatologies, the spatial correlation coefficients of the model runs with E-OBS are all similar (around 0.65), comparable to those of other observational datasets with E-OBS. The model simulations all present similar spatial variances, only slightly higher than that of E-OBS. For comparison, other observational datasets have a significantly smaller variance with a larger spread. In summer (JJA; Fig. 3k) the model runs display a larger spread in variances and correlations, which are comparable with those of other observational datasets. Interestingly, in summer the run at the highest resolution (et04) displays a variance that is identical to that of E-OBS.

We next focus on the precipitation climatology over the GAR subdomain during the years 1979–98, considering the differences between the simulations and EURO4M-APGD (Auer et al. 2007) in Figs. 4a, 4c, and 4e. While run bt11 (Fig. 4c) still displays a wet bias over the GAR domain, run et04 (Fig. 4e) shows better agreement with EURO4M-APGD than run kt11 (Fig. 4a). In particular, excessive precipitation over the French Alps is partially removed and a deficit of precipitation over the Ligurian Apennines is corrected to a large extent. Summer biases over the Alps are particularly sensitive to the convective closure, as shown in Figs. 4b, 4d, and 4f. The Betts–Miller–Janjic convective scheme (Fig. 4d) clearly improves modeling of the rainfall rate over the GAR when compared to run kt11 (Fig. 4b). The high-resolution run et04 (Fig. 4f) presents the highest improvement, significantly reducing the bias over the entire Alpine range.

b. *Annual cycle of precipitation*

Figure 5a shows the monthly climatologies (spatial and temporal averages) of precipitation over the European (IER) domain, limited to land surfaces. Figure 5b shows the same results for the Alpine region (GAR). For the European domain, except for the period June–September, all WRF configurations fall outside the range spanned by the different observational datasets and they significantly overestimate precipitation. In summer, only the high-resolution simulation with explicit convection at 0.037° (et04) manages to significantly reduce the bias and to stay within the observation bounds. A similar behavior is found in the GAR, where all simulations are found to be reasonably close to the observed HISTALP precipitation from September to November. For both domains, the BMJ convection scheme coupled to Thompson microphysics (bt11) is the model configuration at 0.11° providing the best agreement with gridded observational data, particularly in summer and fall.

c. *Daily precipitation statistics and intense precipitation events*

Next we focus on daily precipitation statistics to gauge the capability of the model runs to correctly reproduce the statistics of intense precipitation events.

Figure 6 shows the map of the number of days with rainfall rate larger than 10 mm for E-OBS and for runs kt11, km11, kw11, bt11, and et04 (Figs. 6a–f, respectively). According to E-OBS, frequent heavy precipitation days are essentially localized over the Alps, western Norway, Scotland, and Portugal. This spatial distribution is well captured by the high-resolution run et04. Nevertheless, heavy precipitation days tend to be overestimated by other runs at 0.11° over the Carpathian Mountains, the Pyrenees, and Croatia. For these areas, E-OBS provides estimates of about 40 days yr^{-1} with heavy precipitation, while runs kt11, km11, kw11, and bt11 indicate almost twice this frequency. The simulation kt11 strongly overestimates the number of heavy precipitation days over eastern Europe compared to E-OBS, suggesting that the KF scheme may be overactive.

The distribution of the probabilities of exceedance of precipitation thresholds for the daily rainfall rate on the GAR domain are shown in Fig. 7, for all seasons, for the model results and for EURO4M-APGD.

To allow a fair comparison of the model statistics with the data [the representativeness issue discussed in Kanamitsu and DeHaan (2011)], we also report the distributions for EURO4M-APGD and for the high-resolution experiment et04 aggregated at 0.11°. The curve for the observations aggregated at 0.11° is very close to that at the original resolution (about 5 km), suggesting that the effective resolution of EURO4M-APGD is coarser than its nominal resolution [as also discussed in Isotta et al. (2013)]. In general, we recall that observational datasets can also be affected by uncertainties due to variable station density and measurement

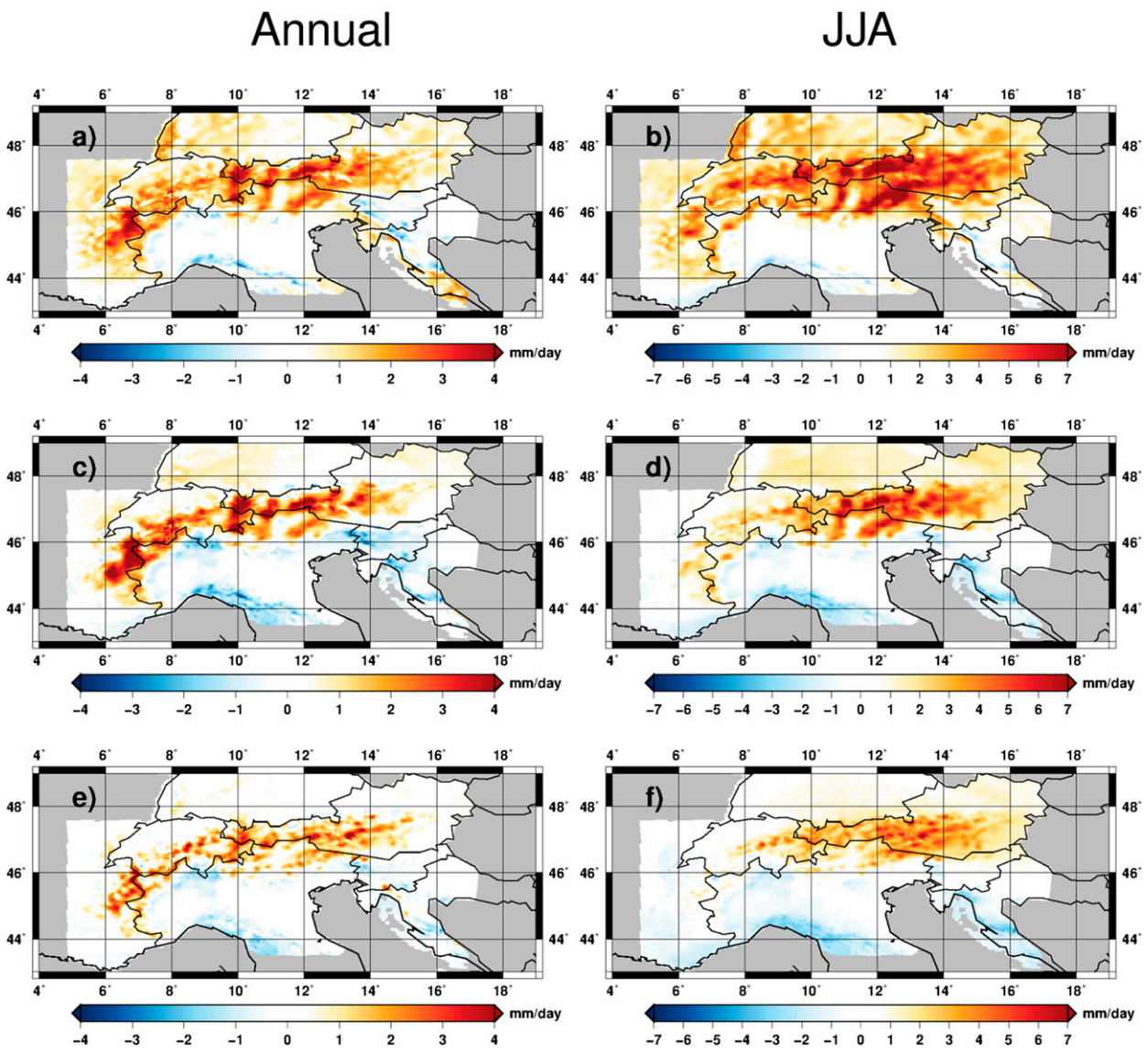

FIG. 4. Differences in the (left) annual and (right) JJA precipitation climatology over the GAR between WRF and EURO4M-APGD for (a),(b) kt11; (c),(d) bt11; and (e),(f) et04.

uncertainties, particularly in high mountain areas, with a possible systematic underestimation of extreme rainfall rates (Isotta et al. 2013).

The comparison of the probabilities of exceedance for the model outputs with those for the observations provides mixed results. The experiment using the BMJ scheme (bt11) reports significantly lower probabilities for extreme precipitation, particularly in summer (JJA), showing that this scheme has difficulties in adequately reproducing intense convective events in summer. Run kw11 (KF and WSM6) successfully reproduces the distributions for all seasons except December–February (DJF), when it severely overestimates the probabilities of exceedance of intense precipitation. The runs using the Morrison scheme (km11) compare well with observations in winter and summer but underestimate the probability of occurrence of intense precipitation in other seasons. A similar behavior is found for the Thompson scheme (kt11), which in winter and summer reproduces the probabilities of observed precipitation up to about 150 mm day^{-1}, while it underestimates the probability of such intense events in other seasons. The high-resolution run (et04) at its original resolution agrees well with observations in most seasons but underestimates the probabilities of intense precipitation (at about >100 mm day^{-1}) when aggregated at 0.11°, except in winter when the aggregated high-resolution run is close to the observations.

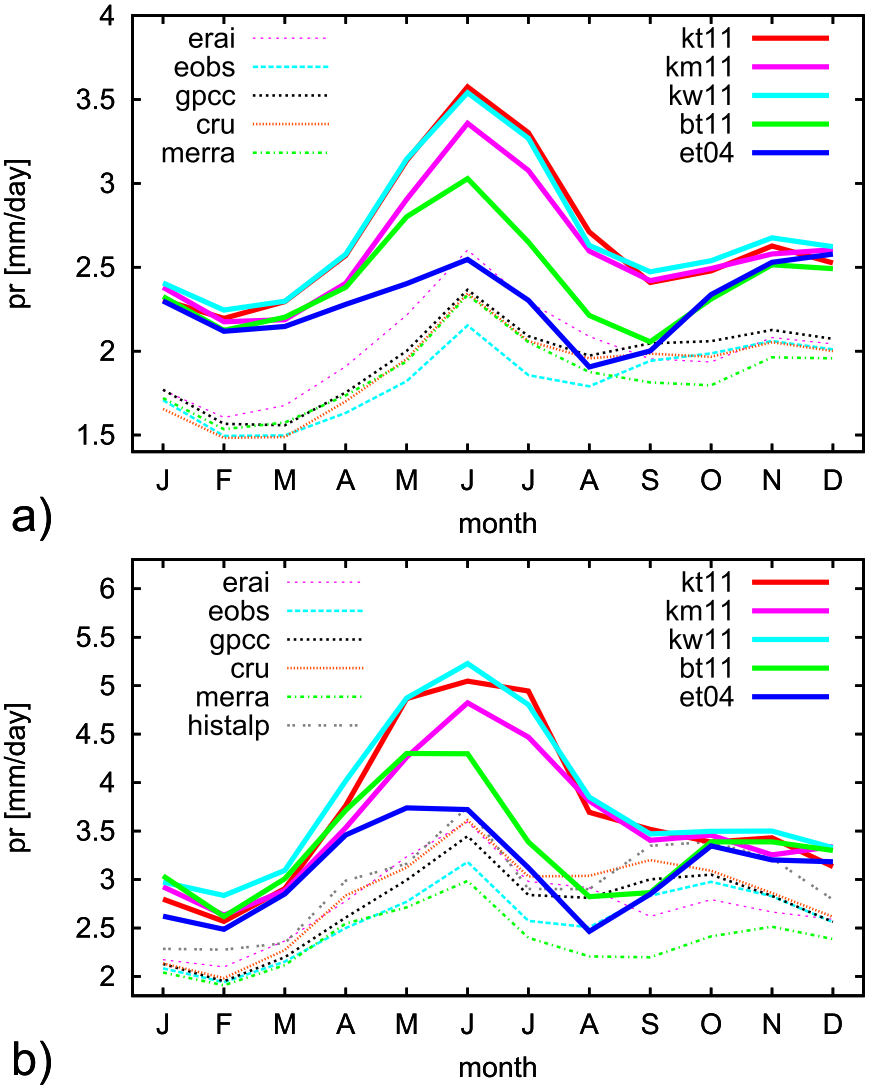

FIG. 5. Monthly precipitation climatologies for 1979–98 averaged over the (a) IER and (b) GAR. A comparison is made between all numerical simulations and the observational data.

Even if our simulations are only constrained by the boundary conditions provided by ERA-Interim, these may be enough to constrain the dynamics to the extent that the daily model fields display significant correlations with observations also at high resolution in the internal parts of the domain. To explore this aspect, we compute the correlation between the daily output of run et04 and EURO4M-APGD (see Fig. 8). Interestingly, the maximum correlation is found in winter (Fig. 8a), spring (Fig. 8b), and fall (Fig. 8d) with correlation coefficients of ~0.4–0.5 on average, with particularly strong correlation over the Alpine range, presumably owing to the strong orographic control of precipitation in such areas. Summer convective events, even if well captured on average, are not in phase with those from EURO4M-APGD, leading to low correlation coefficients (0.24 on average).

5. Discussion and conclusions

Obtaining a realistic, high-resolution representation of precipitation, particularly of intense events, is a necessary prerequisite to develop any reliable assessment of the hydrometeorological risk in future climate change scenarios.

In this work, we analyzed the skill of a high-resolution nonhydrostatic regional climate/meteorological model, the Weather Research and Forecast Model, in representing precipitation over Europe at spatial resolutions 0.11° and 0.037°. To this end, we tested different

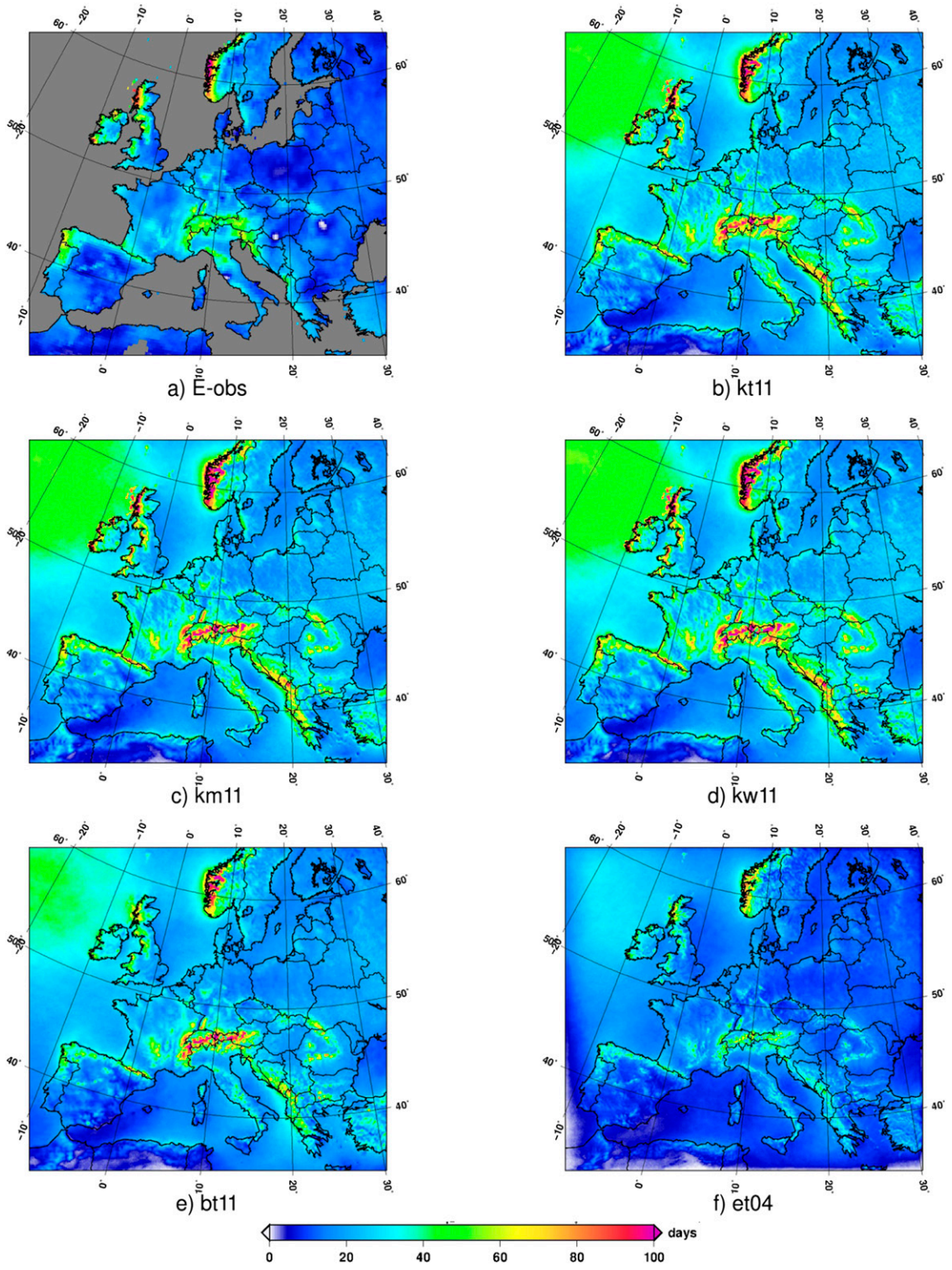

FIG. 6. Number of days with heavy precipitation (>10 mm) for the period 1979–98.

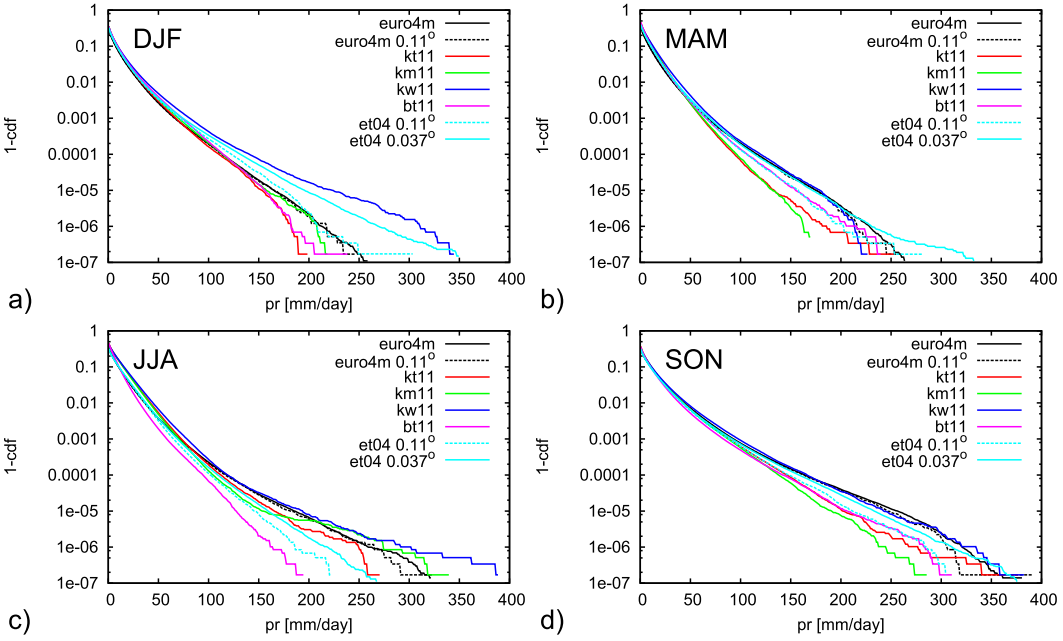

FIG. 7. Exceedance probability for 1979–98 over the GAR, for different WRF simulations and for EURO4M-APGD, for seasons (a) DJF, (b) March–May (MAM), (c) JJA, and (d) September–November (SON). The exceedance probability is computed as 1 minus the precipitation cdf.

standard configurations. In all cases, the WRF Model tends to overestimate precipitation, both in terms of annual average (between 25% and 46% compared to E-OBS) and in terms of localized precipitation extremes, particularly over the Alps. These results are in agreement with Kotlarski et al. (2014), where for models in the European CORDEX ensemble precipitation biases in the range from −40% to +80% were found, with average wet model biases around 30%, particularly in the Alpine region in winter and spring. As also discussed in that reference, a bias around 20% could be justified by uncertainties in the observational datasets. We also find that different gridded observational datasets are characterized by different average precipitation rates, as shown in Table 3, ranging between 1.84 mm day^{-1} (MERRA, E-OBS) and more than 2 mm day^{-1} (ERA-Interim).

Our results show strong sensitivity to the adopted convective scheme, microphysics parameterization, and resolution. The WMS6 microphysics (kw11) best reproduces the probability distribution of precipitation in all seasons, except for winter when it overestimates extreme events. However, this scheme is characterized by a significant average bias. Strong conceptual differences exist between WSM6 and, for example, the Thompson microphysics parameterizations. In particular, we expect WSM6 to better represent convective events as discussed in Otkin et al. (2006). The Thompson scheme tends to produce excessively small droplets and a slow fall speed, implying an underestimated rainfall rate in comparison to WSM6 (Otkin et al. 2006), which could explain the better performance of run kw11 for JJA when the distributions are considered.

When using implicit (parameterized) convection at 0.11°, the Betts–Miller–Janjic scheme provides better results in terms of average precipitation (biases) compared to the Kain–Fritsch scheme in summer, but it still displays a strong overestimation of the rainfall rate over eastern Europe and for regions with complex orography. On the other hand, when the distributions of daily precipitation are considered, BMJ was found to severely underestimate the probability of extreme precipitation rates, particularly in summer. The high-resolution run with explicitly resolved convection presents significantly better performances in terms of bias, particularly over the GAR region, and it better represents the frequency of wet days, but it fails in reproducing the probability of the most intense events in summer.

The ability of the high-resolution simulation in reducing the bias, particularly in summer, may be linked to the fact that the 0.11° resolution falls already close to the gray zone, where convective processes, while not explicitly resolved by the model, are already partially permitted. This may lead to an overrepresentation of convective events, where these are reproduced both explicitly and by the model parameterization, leading to

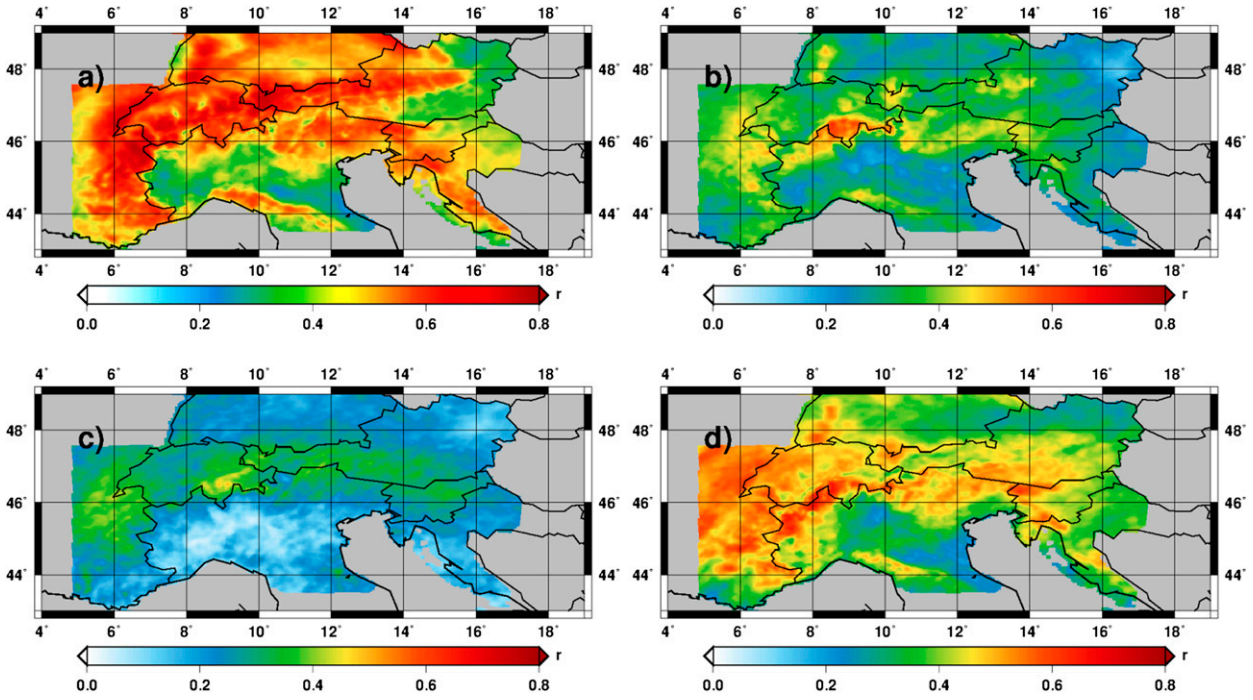

FIG. 8. Correlation of daily precipitation rate for 1979–98 over the GAR between the high-resolution WRF run et04 and EURO4M-APGD, for seasons (a) DJF, (b) MAM, (c) JJA, and (d) SON. The spatial averages of these correlation coefficients are 0.50 (DJF), 0.32 (MAM), 0.24 (JJA), and 0.42 (SON).

excessive triggering of convective precipitation events (Yu and Lee 2010). The fact that the high-resolution simulation better represents the frequency of intense events above 10 mm day^{-1}, as shown both by Figs. 6 and 7, suggests that this mechanism may also be at work here.

The results reported here can be compared with those of Chan et al. (2014), who found that high-resolution simulations over the southern United Kingdom provide a clear added value only for accumulation periods shorter than the daily time scale. This is mainly due to the feature of intense convective events, which develop within a few hours, as reported by observations (Ray et al. 1975; Miller 1975) and numerical simulations (Miglietta and Rotunno 2012). In interpreting these results, we have to consider that most convective closures require the horizontal resolution to be coarser than the size of a single convective cell and are then tuned accordingly. This is true for horizontal resolutions of ~50 km, but this hypothesis may not be true when approaching ~10 km or less. Our results are in line with the findings of Bukovsky and Karoly (2009), who found a strong sensitivity to the convective scheme in studying summer precipitation climatology over North America.

Rasmussen et al. (2011) investigated different model resolutions in the Colorado headwaters region using WRF, concluding that a horizontal resolution of 6 km or less allows us to provide a good reproduction of solid precipitation patterns and a good agreement with observations in winter, focusing on monthly accumulated snowfall. Our results are consistent with this conclusion. As shown in Fig. 8a, daily precipitation from the high-resolution simulation et04 presents high correlation coefficients with observations over the Alpine region in winter, when snowfall largely contributes to precipitation. Figure 7a shows that the model cumulative distribution functions (cdfs) for run et04—aggregated at 0.11°—match the EURO4M-APGD cdfs in DJF. Together, these results confirm the ability of the high-resolution model to reproduce daily precipitation patterns and intensities over complex orography in winter. At the monthly scale, Fig. 5b shows that et04 is the run with the lowest precipitation biases during DJF, in agreement with Rasmussen et al. (2011).

Frei et al. (2006) compared different RCMs from the Prediction of Regional Scenarios and Uncertainties for Defining European Climate Change Risks and Effects (PRUDENCE) project and their ability to predict precipitation statistics for horizontal resolutions ranging from 0.44° to 0.5°. They found that the frequency of wet days is overestimated by most of the RCMs. In our study, this result is confirmed for all runs at 0.11°

horizontal resolution (Figs. 6b–e), while run et04 (Fig. 6f) performs significantly better. They also found large precipitation biases over the Alpine region, ranging from −23% up to +46% for DJF and ranging from −31% up to +20% during JJA. Similarly, in the present study (Tables 3, 4), we find biases ranging from 4% (run et04) up to 28% (run kw11).

Rajczak et al. (2013) compared the skill of various RCMs from the ENSEMBLES project for the period 1971–98 over the Alpine region. This study also reported an overestimation of the frequency of wet days. In agreement with their results, we observe that WRF overestimates heavy precipitation events, particularly in the northern part of the GAR for all 0.11° simulations (Fig. 6). Similar to most models in ENSEMBLES, all our simulations qualitatively capture the precipitation seasonal cycle over the Alpine region (Fig. 5b).

In this work, we focused on the role played by microphysical parameterizations and convective schemes, but we recall that other parameterizations may also have a significant impact on the representation of precipitation in the European domain. For example, Mooney et al. (2013) investigated WRF climatology over Europe for the period 1990–95, forced by ERA-Interim, at the coarser resolution of 0.44°, exploring different longwave radiation schemes, land surface models (LSMs), microphysics schemes, and planetary boundary layer (PBL) schemes. They found strong differences between the precipitation modeled by WRF and the observational datasets, and they found particular sensitivity to the parameters of the LSM during summer, for such coarser model resolutions.

The results reported in this paper are both encouraging and worrisome. On the one hand, it is shown that either increased spatial resolution or appropriate parameterization schemes can provide a better representation of observed precipitation. On the other hand, the cost of running regional climatic simulation at such high resolutions is extremely high, and in any case, there are still severe discrepancies between the numerical results and the observational datasets even at the highest resolution. However, even the reliability of the gridded precipitation data is questionable, and the problem of comparing data and simulations could become difficult to handle. Overall, our results indicate that the best modeling choices seem to vary depending on the chosen metrics, suggesting that different applications may require different model setups.

Acknowledgments. This work was funded by the Project of Interest NextData (MIUR PNR 2011–2013) and by the MIUR PRIN 2010–11 projects ''Innovative methods for water resources management and risk assessment under uncertainty'' and 20108 TZKHC of the Italian Ministry of Education, University and Research. The numerical simulations with the WRF Model used in this study were performed at the LRZ supercomputing center, Garching, Germany, in the framework of the Gauss-EXPRESS project (pr45de). A. Parodi was partially funded by the DRIHM FP7 project. We acknowledge the institutions and the teams responsible for the creation and publication of the GPCC, CRU, HISTALP, EURO4M-APGD, and ERA-Interim archives. ERA-Interim data have been obtained from the ECMWF Data Server. We acknowledge E-OBS from the EU-FP6 project ENSEMBLES (http://ensembles-eu.metoffice.com) and the data providers in the ECA&D project (www.ecad.eu). Finally, A. Parodi acknowledges Prof. Jesus Fernandez (University of Cantabria), who helped in setting up WRF-CLM on the Euro-Cordex domain.

REFERENCES

Auer, I., and Coauthors, 2007: HISTALP—historical instrumental climatological surface time series of the greater alpine region. *Int. J. Climatol.,* **27,** 17–46, doi:10.1002/joc.1377.

Becker, A., P. Finger, A. Meyer-Christoffer, B. Rudolf, K. Schamm, U. Schneider, and M. Ziese, 2013: A description of the global land-surface precipitation data products of the Global Precipitation Climatology Centre with sample applications including centennial (trend) analysis from 1901–present. *Earth Syst. Sci. Data,* **5,** 71–99, doi:10.5194/essd-5-71-2013.

Betts, A. K., 1986: A new convective adjustment scheme. Part I: Observational and theoretical basis. *Quart. J. Roy. Meteor. Soc.,* **112,** 677–691, doi:10.1002/qj.49711247307.

Bukovsky, M. S., and D. J. Karoly, 2009: Precipitation simulations using WRF as a nested regional climate model. *J. Appl. Meteor. Climatol.,* **48,** 2152–2159, doi:10.1175/2009JAMC2186.1.

Castro, C. L., R. A. Pielke, and G. Leoncini, 2005: Dynamical downscaling: Assessment of value retained and added using the Regional Atmospheric Modeling System (RAMS). *J. Geophys. Res.,* **110,** D05108, doi:10.1029/2004JD004721.

Chan, S., E. Kendon, H. Fowler, S. Blenkinsop, N. Roberts, and C. Ferro, 2014: The value of high-resolution met office regional climate models in the simulation of multihourly precipitation extremes. *J. Climate,* **27,** 6155–6174, doi:10.1175/JCLI-D-13-00723.1.

Christensen, J., and O. Christensen, 2003: Climate modelling: Severe summertime flooding in Europe. *Nature,* **421,** 805–806, doi:10.1038/421805a.

Chu, J., K. Warrach-Sagi, V. Wulfmeyer, T. Schwitalla, and H. Bauer, 2010: Regional climate simulation (1989–2009) with WRF in the CORDEX-Europe domain. *EMS Annual Meeting Abstracts,* Vol. 7, Abstract EMS2010-209. [Available online at http://meetingorganizer.copernicus.org/EMS2010/EMS2010-209-1.pdf.]

Dee, D. P., and Coauthors, 2011: The ERA-Interim reanalysis: Configuration and performance of the data assimilation system. *Quart. J. Roy. Meteor. Soc.,* **137,** 553–597, doi:10.1002/qj.828.

Denis, B., R. Laprise, D. Caya, and J. Côté, 2002: Downscaling ability of one-way nested regional climate models: The big-brother experiment. *Climate Dyn.,* **18,** 627–646, doi:10.1007/s00382-001-0201-0.

Flaounas, E., P. Drobinski, M. Vrac, S. Bastin, C. Lebeaupin-Brossier, M. Stéfanon, M. Borga, and J.-C. Calvet, 2013: Precipitation and temperature space–time variability and extremes in the Mediterranean region: Evaluation of dynamical and statistical downscaling methods. *Climate Dyn.,* **40,** 2687–2705, doi:10.1007/s00382-012-1558-y.

Fowler, H. J., and R. L. Wilby, 2010: Detecting changes in seasonal precipitation extremes using regional climate model projections: Implications for managing fluvial flood risk. *Water Resour. Res.,* **46,** W03525, doi:10.1029/2008WR007636.

Frei, C., R. Schöll, S. Fukutome, J. Schmidli, and P. Vidale, 2006: Future change of precipitation extremes in Europe: Intercomparison of scenarios from regional climate models. *J. Geophys. Res.,* **111,** D06105, doi:10.1029/2005JD005965.

Gallus, W. A., Jr., 1999: Eta simulations of three extreme precipitation events: Sensitivity to resolution and convective parameterization. *Wea. Forecasting,* **14,** 405–426, doi:10.1175/1520-0434(1999)014<0405:ESOTEP>2.0.CO;2.

Gerard, L., 2007: An integrated package for subgrid convection, clouds and precipitation compatible with meso-gamma scales. *Quart. J. Roy. Meteor. Soc.,* **133,** 711–730, doi:10.1002/qj.58.

Giorgi, F., 1990: Simulation of regional climate using a limited area model nested in a general circulation model. *J. Climate,* **3,** 941–963, doi:10.1175/1520-0442(1990)003<0941:SORCUA>2.0.CO;2.

——, 2006: Climate change hot-spots. *Geophys. Res. Lett.,* **33,** L08707, doi:10.1029/2006GL025734.

——, and L. O. Mearns, 1991: Approaches to the simulation of regional climate change: A review. *Rev. Geophys.,* **29,** 191–216, doi:10.1029/90RG02636.

——, M. R. Marinucci, and G. Visconti, 1990: Use of a limited-area model nested in a general circulation model for regional climate simulation over Europe. *J. Geophys. Res.,* **95,** 18 413–18 431, doi:10.1029/JD095iD11p18413.

Gobiet, A., and Coauthors, 2012: A new generation of regional climate simulations for Europe: The EURO-CORDEX initiative. *EGU General Assembly Conf.,* Vienna, Austria, EGU, 8211.

Haylock, M. R., N. Hofstra, A. M. G. Klein Tank, E. J. Klok, P. D. Jones, and M. New, 2008: A European daily high-resolution gridded data set of surface temperature and precipitation for 1950–2006. *J. Geophys. Res.,* **113,** D20119, doi:10.1029/2008JD010201.

Hong, S.-Y., and J.-O. J. Lim, 2006: The WRF Single-Moment 6-Class Microphysics Scheme (WSM6). *J. Korean Meteor. Soc,* **42** (2), 129–151.

Isotta, F. A., and Coauthors, 2013: The climate of daily precipitation in the Alps: Development and analysis of a high-resolution grid dataset from pan-Alpine rain-gauge data. *Int. J. Climatol.,* **34,** 1657–1675, doi:10.1002/joc.3794.

Jacob, D., and Coauthors, 2013: Euro-CORDEX: New high-resolution climate change projections for European impact research. *Reg. Environ. Change,* **14,** 563–578, doi:10.1007/s10113-013-0499-2.

Jankov, I., W. A. Gallus, M. Segal, B. Shaw, and S. E. Koch, 2005: The impact of different WRF Model physical parameterizations and their interactions on warm season MCS rainfall. *Wea. Forecasting,* **20,** 1048–1060, doi:10.1175/WAF888.1.

Jones, R. G., J. M. Murphy, and M. Noguer, 1995: Simulation of climate change over Europe using a nested regional-climate model. I: Assessment of control climate, including sensitivity to location of lateral boundaries. *Quart. J. Roy. Meteor. Soc.,* **121,** 1413–1449, doi:10.1002/qj.49712152610.

Kain, J. S., and J. M. Fritsch, 1990: A one-dimensional entraining/detraining plume model and its application in convective parameterization. *J. Atmos. Sci.,* **47,** 2784–2802, doi:10.1175/1520-0469(1990)047<2784:AODEPM>2.0.CO;2.

——, S. J. Weiss, J. J. Levit, M. E. Baldwin, and D. R. Bright, 2006: Examination of convection-allowing configurations of the WRF Model for the prediction of severe convective weather: The SPC/NSSL spring program 2004. *Wea. Forecasting,* **21,** 167–181, doi:10.1175/WAF906.1.

——, and Coauthors, 2008: Some practical considerations regarding horizontal resolution in the first generation of operational convection-allowing NWP. *Wea. Forecasting,* **23,** 931–952, doi:10.1175/WAF2007106.1.

Kanamitsu, M., and L. DeHaan, 2011: The Added Value Index: A new metric to quantify the added value of regional models. *J. Geophys. Res.,* **116,** D11106, doi:10.1029/2011JD015597.

Kotlarski, S., and Coauthors, 2014: Regional climate modeling on European scales: A joint standard evaluation of the EURO-CORDEX RCM ensemble. *Geosci. Model Dev. Discuss.,* **7,** 217–293, doi:10.5194/gmdd-7-217-2014.

Lo, J. C.-F., Z.-L. Yang, and R. A. Pielke, 2008: Assessment of three dynamical climate downscaling methods using the Weather Research and Forecasting (WRF) Model. *J. Geophys. Res.,* **113,** D09112, doi:10.1029/2007JD009216.

McGregor, J. L., 1997: Regional climate modelling. *Meteor. Atmos. Phys.,* **63,** 105–117, doi:10.1007/BF01025367.

Miglietta, M., and R. Rotunno, 2012: Application of theory to simulations of observed cases of orographically forced convective rainfall. *Mon. Wea. Rev.,* **140,** 3039–3053, doi:10.1175/MWR-D-11-00253.1.

Miller, L., 1975: Internal airflow of a convective storm from dual-Doppler radar measurements. *Pure Appl. Geophys.,* **113,** 765–785, doi:10.1007/BF01592958.

Mitchell, T. D., and P. D. Jones, 2005: An improved method of constructing a database of monthly climate observations and associated high-resolution grids. *Int. J. Climatol.,* **25,** 693–712, doi:10.1002/joc.1181.

Mooney, P. A., F. J. Mulligan, and R. Fealy, 2013: Evaluation of the sensitivity of the weather research and forecasting model to parameterization schemes for regional climates of Europe over the period 1990–95. *J. Climate,* **26,** 1002–1017, doi:10.1175/JCLI-D-11-00676.1.

Morrison, H., and A. Gettelman, 2008: A new two-moment bulk stratiform cloud microphysics scheme in the Community Atmosphere Model, version 3 (CAM3). Part I: Description and numerical tests. *J. Climate,* **21,** 3642–3659, doi:10.1175/2008JCLI2105.1.

Murphy, J., 2000: Predictions of climate change over Europe using statistical and dynamical downscaling techniques. *Int. J. Climatol.,* **20,** 489–501, doi:10.1002/(SICI)1097-0088(200004)20:5<489::AID-JOC484>3.0.CO;2-6.

New, M., M. Hulme, and P. Jones, 1999: Representing twentieth-century space–time climate variability. Part I: Development of a 1961–90 mean monthly terrestrial climatology. *J. Climate,* **12,** doi:10.1175/1520-0442(1999)012<0829:RTCSTC>2.0.CO;2.

——, ——, and ——, 2000: Representing twentieth-century space–time climate variability. Part II: Development of 1901–96 monthly grids of terrestrial surface climate. *J. Climate,* **13,** doi:10.1175/1520-0442(2000)013<2217:RTCSTC>2.0.CO;2.

Otkin, J. A., H.-L. Huang, and A. Seifert, 2006: A comparison of microphysical schemes in the WRF Model during a severe

weather event. Preprints, *7th Annual WRF User's Workshop,* Boulder, CO, UCAR, 5 pp. [Available online at http://www2.mmm.ucar.edu/wrf/users/workshops/WS2006/abstracts/PSession05/P5_7_Otkin.pdf.]

Palazzi, E., J. von Hardenberg, and A. Provenzale, 2013: Precipitation in the Hindu-Kush Karakoram Himalaya: Observations and future scenarios. *J. Geophys. Res. Atmos.,* **118,** 85–100, doi:10.1029/2012JD018697.

Prein, A. F., G. J. Holland, R. M. Rasmussen, J. Done, K. Ikeda, M. P. Clark, and C. H. Liu, 2013: Importance of regional climate model grid spacing for the simulation of heavy precipitation in the Colorado headwaters. *J. Climate,* **26,** 4848–4857, doi:10.1175/JCLI-D-12-00727.1.

Rajczak, J., P. Pall, and C. Schär, 2013: Projections of extreme precipitation events in regional climate simulations for Europe and the Alpine region. *J. Geophys. Res. Atmos.,* **118,** 3610–3626, doi:10.1002/jgrd.50297.

Rasmussen, R., and Coauthors, 2011: High-resolution coupled climate runoff simulations of seasonal snowfall over Colorado: A process study of current and warmer climate. *J. Climate,* **24,** 3015–3048, doi:10.1175/2010JCLI3985.1.

Ray, P., R. Doviak, G. Walker, D. Sirmans, J. Carter, and B. Bumgarner, 1975: Dual-Doppler observation of a tornadic storm. *J. Appl. Meteor.,* **14,** 1521–1530, doi:10.1175/1520-0450(1975)014<1521:DDOOAT>2.0.CO;2.

Rebora, N., L. Ferraris, J. von Hardenberg, and A. Provenzale, 2006: Rainfall downscaling and flood forecasting: a case study in the Mediterranean area. *Nat. Hazards Earth Syst. Sci.,* **6,** 611–619, doi:10.5194/nhess-6-611-2006.

Rienecker, M. M., and Coauthors, 2011: MERRA: NASA'S Modern-Era Retrospective Analysis for Research and Applications. *J. Climate,* **24,** 3624–3648, doi:10.1175/JCLI-D-11-00015.1.

Roe, G. H., 2005: Orographic precipitation. *Annu. Rev. Earth Planet. Sci.,* **33,** 645–671, doi:10.1146/annurev.earth.33.092203.122541.

Rotunno, R., and R. A. Houze, 2007: Lessons on orographic precipitation from the mesoscale Alpine programme. *Quart. J. Roy. Meteor. Soc.,* **133,** 811–830, doi:10.1002/qj.67.

Saha, S., and Coauthors, 2010: The NCEP Climate Forecast System Reanalysis. *Bull. Amer. Meteor. Soc.,* **91,** 1015–1057, doi:10.1175/2010BAMS3001.1.

Skamarock, W. C., J. B. Klemp, J. Dudhia, D. O. Gill, D. M. Barker, W. Wang, and J. G. Powers, 2005: A description of the Advanced Research WRF version 2. NCAR Tech. Note NCAR/TN-468+STR, 88 pp., doi:10.5065/D6DZ069T.

Thompson, G., R. M. Rasmussen, and K. Manning, 2004: Explicit forecasts of winter precipitation using an improved bulk microphysics scheme. Part I: Description and sensitivity analysis. *Mon. Wea. Rev.,* **132,** 519–542, doi:10.1175/1520-0493(2004)132<0519:EFOWPU>2.0.CO;2.

Vannitsem, S., and F. Chomé, 2005: One-way nested regional climate simulations and domain size. *J. Climate,* **18,** 229–233, doi:10.1175/JCLI3252.1.

Wang, W., 2011: An assessment of the surface climate in the NCEP climate forecast system reanalysis. *Climate Dyn.,* **37,** 1601–1620, doi:10.1007/s00382-010-0935-7.

——, and N. L. Seaman, 1997: A comparison study of convective parameterization schemes in a mesoscale model. *Mon. Wea. Rev.,* **125,** 252–278, doi:10.1175/1520-0493(1997)125<0252:ACSOCP>2.0.CO;2.

Warrach-Sagi, K., T. Schwitalla, V. Wulfmeyer, and H.-S. Bauer, 2013: Evaluation of a climate simulation in Europe based on the WRF–Noah Model system: Precipitation in Germany. *Climate Dyn.,* **41,** 755–774, doi:10.1007/s00382-013-1727-7.

Wilson, C. A., and J. F. B. Mitchell, 1987: Simulated climate and CO_2-induced climate change over Western Europe. *Climatic Change,* **10,** 11–42, doi:10.1007/BF00140555.

Yu, X., and T.-Y. Lee, 2010: Role of convective parameterization in simulations of a convection band at grey-zone resolutions. *Tellus,* **62A,** 617–632, doi:10.1111/j.1600-0870.2010.00470.x.